

# Lunar Pole Illumination and Communications Maps Computed from GSSR Elevation Data

Scott Bryant  
California Institute of Technology  
Jet Propulsion Laboratory  
4800 Oak Grove Drive  
Pasadena, CA 91109  
818-354-5979  
scott.bryant@jpl.nasa.gov

*Abstract*—A Digital Elevation Model of the lunar south pole was produced using Goldstone Solar System RADAR (GSSR) data obtained in 2006.<sup>12</sup> This model has 40-meter horizontal resolution and about 5-meter relative vertical accuracy [Ref 1]. This Digital Elevation Model was used to compute average solar illumination and Earth visibility with 100 km of the lunar south pole. The elevation data were converted into local terrain horizon masks, then converted into lunar-centric latitude and longitude coordinates. The horizon masks were compared to latitude, longitude regions bounding the maximum Sun and Earth motions relative to the moon. Estimates of Earth visibility were computed by integrating the area of the region bounding the Earth’s motion that was below the horizon mask. Solar illumination and other metrics were computed similarly. Proposed lunar south pole base sites were examined in detail, with the best site showing yearly solar power availability of 92% and Direct-To-Earth (DTE) communication availability of about 50%. Similar analysis of the lunar south pole used an older GSSR Digital Elevation Model with 600-meter horizontal resolution. The paper also explores using a heliostat to reduce the photovoltaic power system mass and complexity.

## TABLE OF CONTENTS

<b>1. INTRODUCTION</b> .....	<b>1</b>
<b>2. BACKGROUND</b> .....	<b>2</b>
<b>3. ANALYSIS METHOD</b> .....	<b>2</b>
<b>4. RESULTS</b> .....	<b>5</b>
<b>5. CONCLUSIONS</b> .....	<b>10</b>
<b>6. ACKNOWLEDGMENTS</b> .....	<b>10</b>
<b>7. REFERENCES</b> .....	<b>10</b>
<b>8. BIOGRAPHY</b> .....	<b>11</b>

## 1. INTRODUCTION

The moon’s rotation pole is inclined 1.54 degrees to the Ecliptic pole. This means the Sun never rises more than a few degrees above the horizon in the lunar Polar Regions. Many depressions and crater floors near the poles are permanently shaded from the Sun, producing permanent low-temperature areas. These permanently shaded areas may be reservoirs for water ice deposits [Ref 2]. The potential for using lunar ice to produce oxygen, hydrogen fuel, and drinking water is driving investigations of human exploration bases at the lunar poles [Ref 3].

The same geometry that creates permanently shadowed lunar polar craters also increases solar illumination on lunar polar mountains. A typical lunar surface location is exposed to the Sun for half of the 29.5-day synodic month. But a tall peak near the lunar poles could view the Sun during the entire synodic month. These “Peaks of Eternal Light” [Ref 4] would provide base sites with near-continuous solar power and illumination [Ref 5, 6]. The analysis presented here shows no Peak of Eternal Light at either lunar pole, but shows several locations with more than 90% solar illumination average over the lunar year.

Evaluating the resource potential of lunar polar base sites is a high priority for future lunar exploration [Ref 7]. This includes determining the amount of Direct-To-Earth communications available from the polar base locations. The orbital mechanics causing the lunar librations seen from Earth also cause the Earth to move several degrees of elevation and azimuth in the lunar sky. Even though the moon is tidally locked, the Earth appears to move  $\pm 6.87$  degrees in latitude and  $\pm 8.16$  degrees in longitude<sup>3</sup>. Therefore, lunar polar base DTE communications is only possible about half of each sidereal month (27.3 days). This paper presents averages of solar illumination, solar power, and Earth visibility metrics for the lunar Polar Regions to help evaluate potential base sites.

<sup>1</sup> 978-1-4244-2622-5/09/\$25.00 ©2009 IEEE.

<sup>2</sup> IEEEAC paper #1659, Version 2, Updated January 26, 2009

<sup>3</sup> R. Roncoli, “Lunar Constants and Models Document”, JPL D-32296, Sept 23, 2005.

## 2. BACKGROUND

The latest Digital Elevation Model from the Goldstone Solar System RADAR (GSSR) was produced from observations taken during September 2006. The GSSR uses antennas in NASA's Deep Space Network to produce RADAR images of solar system objects [Ref 1] using interferometry techniques. These data were acquired during lunar librations that increased the view of the lunar south pole. The Earth's selenographic latitude was -6.2 degrees, allowing the GSSR to see lunar terrain covering out to 70 km toward the Farside of the lunar south pole. The RADAR data was processed into a Digital Elevation Model in polar stereographic projection coordinates. The Digital Elevation Model covers an area approximately 880 km from Nearside to Farside and 500 km East to West across the lunar south pole.

The Digital Elevation Model uses a polar stereographic Cartesian coordinate system centered on the lunar south pole, with X-axis pointed East (90 degrees lunar East Longitude), and Y-axis pointed Nearside (0 degrees lunar East Longitude). Figure 1 shows the lunar south pole region of the 2006 Digital Elevation Model data, along with some lunar features. The lunar south pole is on the rim of Shackleton crater. Figure 2 shows the lunar north pole region of the 1997 Digital Elevation Model data, with some lunar features. The gray areas in both figures were not visible from the Earth during the RADAR imaging. Both figures show two-letter designations of base sites used in this paper. Most features names and locations are from the International Astronomical Union (IAU) lunar naming [Ref 8], however some of the mountain peaks use older, unofficial names [Ref 9].

Figure 3 shows the lunar south pole base locations around Shackleton crater. The figure reveals the high resolution of the south pole RADAR Digital Elevation Model. The 40-meter spatial resolution of the data produces a topographic map with good internal consistency and rich detail. Inside Shackleton crater, the missing elevation data within the RADAR shadow were filled in with values based on a parabolic elevation profile. Figure 3 also shows the rim of Shackleton crater covers a horizontal distance of about 200 meters (5 data points), instead of being an abrupt scarp. This suggests the actual Digital Elevation Model point-to-point elevation error is close to the stated relative vertical accuracy of 5 meters [Ref 1]. Based on this vertical accuracy, the analysis used 2-meter tall towers for the baseline horizon mask computations.

## 3. ANALYSIS METHOD

Analyzing the Digital Elevation Model to produce solar illumination and DTE communications required several major steps. Step 1 corrected the Digital Elevation Model elevations, by removing bad points and filling in RADAR shadow areas with approximate elevations. Step 2

computed horizon masks from the Digital Elevation Model information. Topocentric horizon masks were computed for a 2 meter altitude above the surface, and then converted into lunar-centered equatorial latitude and longitude coordinates. Step 3 computed illumination metrics by projecting the horizon mask in lunar equatorial latitude and longitude onto the celestial sphere. The horizon mask was then compared to the average motions of the Sun and Earth. This step assumed a simplified time-average for the solar and Earth motions as seen from the moon, eliminating the astrodynamics calculations. Solar illumination and DTE visibility metrics were computed by integrating along the horizon mask in the lunar-centered latitude and longitude coordinates. Step 4 collected these illumination and DTE visibility metrics for areas around the lunar poles. Those metrics were captured as contour plots and tables.

### *Step 1: Digital Elevation Model Corrections and Filling*

During the 2006 GSSR data acquisition, the Earth was at -6.2 degrees selenographic latitude. This placed Earth at approximately +6.2 degrees of elevation angle as seen from the lunar south pole, so parts of the polar terrain were not visible to the RADAR. For the 100 km x 100 km area centered on the lunar south pole, about 40% of the area was not imaged because it was in RADAR shadow. In addition, several areas that were imaged had very low RADAR backscatter signal strength, leading to spurious elevation values. In several locations next to the RADAR shadow edge, the algorithms for processing RADAR phase into elevation data produced erroneous elevation values. These features of the GSSR Digital Elevation Model required correction prior to using the Digital Elevation Model for illumination computations.

The 2006 GSSR Digital Elevation Model file of elevations and the file of backscatter magnitudes were read into Matlab. Because of the large file size, the program read a data subset covering 100 km x 100 km area at full 40-meter resolution (2501 x 2501 pixels) centered on the lunar south pole. For coarser far-field computations, the program read in a 400 km x 400 km area and decimated it to 600-meter resolution by taking every 15<sup>th</sup> point (667 x 667 pixels). The program then edited the Digital Elevation Model elevations to remove known artifacts. Specifically, the areas (-8.5 km < X < -7 km, -14.5 km < Y < -13.5 km) and (-7 km < X < -3 km, -16 km < Y < -12 km) were scanned and all elevations greater than 800 meters were set to the value of the RADAR shadow areas (-10,000 meters). This removed 2 steep-sided 'towers' or 'spikes' in elevation data on a ridgeline west of Shackleton crater. GSSR experts at JPL confirmed these 2 'towers' were probably anomalies from the processing algorithms. The remaining area was 6,180 km<sup>2</sup>, or 61.8% of the 100 km x 100 km original area.

The Matlab program then pruned out elevations with local slopes in excess of 60 degrees. Slopes greater than 60 degrees are physically unrealistic and are probably artifacts of the RADAR processing. For the 100 km x 100 km area

centered on the lunar south pole, this removed 1.7% of the remaining elevation area. Next the program removed elevation points with RADAR backscatter value less than 0.06%, removed 18.3% of the remaining elevation area. Several elevation anomalies were eliminated by this backscatter limit, including hilly terrain inside the nearside-east rim of Shackleton crater. This hilly terrain was explained as a processing artifact, because it would have obscured the Earth's view of other RADAR-imaged terrain inside Shackleton crater.

The Matlab program then scanned the remaining elevation values and removed any points with less than 4 surrounding points. This removed almost all small 'islands' of elevation data, which were artifacts of the RADAR processing. This step removed 0.5% of the elevation data. The cumulative effect of the data editing removed about 21% of the original elevation data. This reduced the elevation data in the referenced 100 km x 100 km area from 6180 km<sup>2</sup> to 4916 km<sup>2</sup> or from 61.8% to 49.2% of the mapped area. Similar percentages were removed for the larger coarse maps.

The Matlab program then created elevation data to fill in the missing points. Inside Shackleton crater, the program created a parabolic surface with a center elevation of -2900 meters at X = 7.32 km, Y = -8.08 km. This produced a more realistic three-dimensional plot of the crater, but did not affect the illumination results. For the remaining RADAR shadow and edited areas, the program set the elevation value to the altitude of the RADAR shadow. The program scanned each column of elevation data from the +Y to -Y direction. At each missing data location, the program computed a straight line from Earth at -6.2 degrees selenographic latitude that passed through the last known +Y elevation data value. This means the elevation in the unknown terrain was set to values just under the GSSR RADAR shadow envelope. This models an upper bound on the possible elevations. If the actual elevations were higher, then the point would have appeared on the RADAR. This upper bound provides a conservative estimate for solar illumination computations. Actual terrain elevations inside the RADAR shadow area are probably lower than the RADAR line of sight, and would block less of the surrounding terrain. The program also set a lower limit of -5000 meters elevation to prevent elevation estimates toward the lunar Farside from getting excessively deep.

Similar pruning was applied to the lunar south pole Digital Elevation Model from 1997. The program read in a 400 km x 400 km area at the 600-meter resolution of the Digital Elevation Model. The same data pruning algorithms were applied, but no specific elevation artifacts were targeted for removal.

### *Step 2: Horizon Mask Computation*

The horizon masks were computed by scanning along lines of constant azimuth. For convenience in computation, the line of 0 azimuth was always parallel to the lunar prime

meridian at 0 degree longitude, not due North. This made the conversion to the final equatorial coordinates easier and did not affect the results. Maps were selected with "coarse" or "fine" grid resolution, described below. For each point on the grid, the Matlab program scanned along lines of azimuth for at least 200 km. This 200 km distance was determined from a requirement to examine far enough along the azimuth lines to find any peaks that would block the Sun. At mid-Winter, the Sun's elevation is -1.54 degrees as seen from the lunar south pole. The tallest peak near the south pole is Leibnitz  $\beta$ , with elevation 6055 meters. Figure 4 shows how the lunar horizon falls off quickly with distance. At 200 km from the pole, a mountain must be over 7000 meters tall in order to block the Winter Sun. This gave a practical limit of 200 km for the distance to use when scanning along the lines of azimuth. This also set the size necessary for the Digital Elevation Model subset maps.

The elevation angles were computed starting with the grid point at the center of the horizon mask and extending out to points on the lunar terrain along each azimuth line. The maximum elevation angle for each azimuth was stored in an array of horizon mask elevation versus azimuth. The horizon mask results depend on the altitude of the center of the horizon mask above the local terrain. Unless otherwise stated, a tower 2 meters above the local terrain was used for the horizon mask computations. This represented a practical height for solar array installation. For some locations, horizon mask metrics were computed using taller towers.

Coarse resolution horizon masks were computed from a Digital Elevation Model decimated to 600-meter spatial resolution that extended  $\pm 200$  km around the lunar south pole. The lines of azimuth were spaced 5 degrees apart. Maps were generated covering 30 km x 30 km areas (51 by 51 pixels). A total of 64 maps were generated to cover the region within 110 km of the lunar south pole. For the lunar north pole, maps were generated in the same way. Because there are no extremely tall mountains to consider near the lunar north pole, fewer maps were examined. A total of 42 maps were generated, covering the regions within 105 km of the lunar north pole, except the farside which was covered to 75 km.

For the lunar south pole, medium resolution horizon masks were computed for specific areas of interest. The medium resolution masks used 2 Digital Elevation Models: a coarse Digital Elevation Model decimated to 1000-meter spatial resolution that extended  $\pm 200$  km around the lunar south pole, and a fine Digital Elevation Model at 40-meter spatial resolution that extended  $\pm 6$  km around the location of interest. This 12 km x 12 km area was removed from the coarse Digital Elevation Model prior to the elevation angle computations. Horizon masks were computed for both Digital Elevation Models, using azimuth spacing of 5 degrees. Then for each azimuth, the greater elevation angle of the 2 horizon masks was selected for the composite horizon mask. This 2 Digital Elevation Model approach produced a higher resolution result, while keeping the

computation time reasonably short. Maps were generated covering 1 km x 1 km areas with resolution of 40 meters (51 by 51 pixels).

For a small number of locations, fine resolution horizon masks were computed using 2 Digital Elevation Models: a coarse Digital Elevation Model decimated to 1000 meter spatial resolution that extended  $\pm 200$  km around the lunar south pole, and a fine Digital Elevation Model at 40 meter spatial resolution that extended  $\pm 50$  km around the lunar south pole. This 100 km x 100 km area was removed from the coarse Digital Elevation Model prior to the elevation angle computations. Horizon masks were computed for both Digital Elevation Models, using azimuth spacing of 1 degree. Then for each azimuth, the greater elevation angle of the 2 horizon masks was selected for the composite horizon mask. This 2 Digital Elevation Model approach produced a higher resolution result, while keeping the computation time reasonably short. Horizon masks were computed for single point locations, and extra solar illumination and Earth visibility metrics were created from the horizon masks. The fine resolution computations were performed only at optimal solar illumination locations found from the coarse and medium resolution maps.

### *Step 3: Computing Illumination Metrics from Average Solar and Earth Motion*

Figure 5 shows a horizon mask profile in lunar topographic azimuth and elevation coordinates. This mask was produced with 1-degree azimuth steps using the ‘Fine’ resolution technique described above. The figure shows areas defining the limits for the Earth and solar motion, as seen from the moon. The Earth is confined to a maximum east-west longitude libration of 8.16 degrees, and a north-south latitude libration of 6.87 degrees<sup>3</sup>. These librations values are the maximum possible librations, not the typical average values. The motion of the Earth’s center is shown by the parallelogram marked with red circles. The Earth’s disk subtends an angle of 1.9 degrees, as seen from the moon. The motion of the Earth’s South Pole is shown by the parallelogram marked with red dots.

The Sun moves across all degrees of longitude, but is confined to latitudes between 1.54 degrees north and south. The motion of the Sun’s center is plotted with yellow circles. The solar disk subtends an angle of 0.53 degrees, as seen from the moon. The motions of the northern and southern limbs of the Sun are shown with yellow lines. The Sun’s path is lowest on the horizon toward the lunar south pole, at azimuth =  $\arctan(x/y)$  or 42.2 degrees.

Figure 6 shows the same information as Figure 5, but transferred to lunar equatorial coordinates. In the equatorial frame, the Earth and Sun maximum limits are defined by rectangles. The lunar terrain horizon mask has shifted with this coordinate transformation, raising up in the direction of the lunar south pole at 42.2 degrees longitude, and dipping

down in the direction of the lunar north pole at -137.8 degrees longitude.

The following assumptions were made to simplify the solar illumination and Earth visibility computations:

- 1) The Sun and Earth stay within the bounding rectangles. The center of the solar disk stays within a rectangle defined by east-west longitudes 180 degrees, and north-south latitudes of 1.54 degrees. The center of Earth’s disk stays within east-west longitudes 8.16 degrees, and north-south latitudes 6.87 degrees.
- 2) Averaged over many years, the Sun and Earth motions bring them to all locations within their bounding rectangles. Particularly, during the 18.6-year period of the regression of the longitude of the ascending node, the Earth will cover all locations within its bounding rectangle.
- 3) Averaged over many years, the Sun has an equal probability at being at any location within its bounding rectangle. A similar assumption is made for the Earth within its bounding rectangle. This assumption is less accurate for the Earth, since the Earth does not reach the extremes of latitude libration in every year.

These assumptions bypass computing the exact location of the Sun and Earth at specific times of interest. Instead, average illumination was computed using the area of the bounding rectangles in Figure 6. Illumination metrics are proportional to amount the bounding rectangle area not covered by the terrain horizon mask. The assumptions mean that the illumination metrics will not be exact for a particular date, but represent a multi-year average value. These averaged values allow accurate comparisons between different lunar sites, since the only variable is the lunar terrain at the different locations. These assumptions greatly reduced the amount of computation needed for computing illumination and Earth visibility metrics.

### *Step 4: Solar Illumination and DTE Visibility Metrics*

Based on the assumptions above, several metrics were computed from horizon masks projected into the lunar equatorial coordinates. Average solar illumination was computed by integrating the area of the Sun’s bounding rectangle above the horizon mask. The integrated area was then normalized with the area of the entire solar bounding rectangle, resulting in the percentage of an average year that the Sun is visible. Three types of solar illumination averages were computed, varying with the amount of visible solar disk (see Figure 6). Since the solar disk radius is 0.265 degrees as seen from Earth’s orbit, the metrics vary with the amount of the solar disk covered.

The “0% of solar disk visible” is the average computed by integrating the horizon mask over the solar bounding rectangle from -1.275 degrees +1.805 degrees latitude (for convenience, each pole was treated as the North pole where positive latitudes convert to higher elevations above the local horizon). This bounding rectangle covers the Sun’s limb that is highest above the local horizon. This metric

requires that the horizon mask cover the entire solar disk, up to the higher solar limb, to not be counted in the yearly average of illuminating the lunar terrain. This metric is the percent of time that any solar light is available; no matter how small a section of the solar disk is visible.

The “50% of solar disk visible” metric integrated the horizon mask over the solar bounding rectangle from -1.54 degrees +1.54 degrees latitude. This metric requires that the horizon mask cover half the solar disk to not count as illuminating the lunar terrain. This metric represents half-strength solar illumination.

The “100% of solar disk visible” metric integrated the horizon mask over the solar bounding rectangle from -1.805 degrees to +1.275 degrees latitude. This metric requires that the horizon mask merely touch the solar disk at the lower limb, to not count as illuminating the lunar terrain. This 100% metric is the percentage of the year with full solar power available.

The three types of Earth illumination averages were computed in a similar way. The “0% of Earth visible” average integrated the horizon mask over the Earth bounding rectangle from -5.92 degrees +7.82 degrees latitude. This metric requires that the horizon mask cover the entire Earth disk to not count as visible to the lunar terrain. The 0% metric is the percentage of the year with some part of the Earth visible.

The “50% of Earth visible” average integrated the horizon mask over the Earth bounding rectangle from -6.87 degrees +6.87 degrees latitude. This metric requires that the horizon mask cover half the Earth’s disk to not count as visible. For the lunar south pole, this metric is the amount of time that the Earth’s southern hemisphere is visible.

The “100% of Earth visible” average integrated the horizon mask over the Earth bounding rectangle from -7.82 degrees to +5.92 degrees latitude. This metric requires that the horizon mask merely touch the Earth’s disk to not count as visible. This 100% metric is the percentage of the year with a full Earth visible.

Additional metrics were computed for solar power characterization. The “months 100% visible” gives the number of synodic months per year when the specified percentage of solar disk is visible. It was computed by comparing the maximum horizon mask peak latitude to the upper and lower solar bounding rectangle limits. If the maximum peak reached across 2/3 of the rectangle, then 1/3 of the year has continuous illumination.

The metric “days dark in winter month” is the number of days during the lunar south pole Winter with less than the specified percentage of solar disk visible. This was computed by finding the amount of each solar rectangle lower boundary edge that was below the horizon mask, normalizing with 360 degrees, and multiplying by 29.53

days. For the “100% of solar disk visible” rectangle, this metric is the sum of the number of days without full solar power during the winter synodic month. For the “0% of solar disk visible” metric, this is the sum of the days without any solar light during the winter synodic month. This metric and the “days longest darkness” do not consider possible solar eclipses, which last up to 3.9 hours for a partial eclipse [Ref 6].

The metric “days longest darkness” is the longest continuous period with less than the specified percentage of solar disk visible. For the “100% of solar disk visible” value, this metric is the longest continuous period without full solar power. For the “0% of solar disk visible” value, this metric is the longest continuous period without any solar light. The metric was computed by finding the longest continuous stretch of a solar rectangle lower boundary edge that was below the horizon mask, normalizing with 360 degrees, and multiplying by 29.53 days.

The metrics “days dark in winter month” and “days longest darkness” can be used to set upper and lower bounds on a lunar base power system battery storage requirements. For a worst-case number that ignores recharge rates, battery storage can be based on the “days dark in winter month” value associated with “100% of solar disk visible”. Table 2 shows examples of these metrics.

## 4. RESULTS

Results were assembled in graphical and tabular formats. Contour plots from the coarse (600 meter resolution) horizon mask results were produced for the lunar south pole region. These Coarse maps cover the region from X, Y = -129 km, -114 km to X, Y = +111 km, +126 km in 64 maps that are 30 km x 30 km, and show yearly average solar illumination and Earth communications values (see Figures 7 and 8). The boundaries for the Coarse maps were chosen so that the entire Shackleton crater fit within the Coarse map from X, Y = -9 km, -24 km to X, Y = +21 km, +6 km.

For the lunar north pole region, coarse maps cover from X, Y = -105 km, -105 km to X, Y = +105 km, +75 km. Figures 9 and 10 show yearly average solar illumination and Earth communications visibility values.

For both lunar poles, solar illumination peaks were tabulated from the coarse maps and compared to illumination peak sites in the references. For the lunar south pole, coarse map sites with more than 80% average solar illumination were then examined with Medium resolution maps covering areas 2 km x 2 km. The Medium resolution maps were used to determine the size of each site in 40 m x 40 m pixels. The location of maximum solar illumination in X and Y was then determined for each site. These “peaks of illumination” were then examined with the Fine horizon

mask analysis to verify the illumination results and produce additional metrics.

### Coarse Horizon Mask Results

For the south pole region, only 5 of the 64 coarse (30 km x 30 km) maps have peaks with more than 80% average solar illumination. These 5 maps cover Shackleton crater and the lunar south pole, the east ridge from Shackleton crater, the west ridge from Shackleton crater, The nearside-east rim of de Gerlache crater, and the nearside rim of de Gerlache crater.

The maps confirm that most of Shackleton crater is in permanent shadow (see figure 7). The contours of solar illumination show small areas of maximum illumination on Shackleton crater's rim and the West Ridge. The maximum is around 90% yearly average solar illumination. The contours of Earth illumination show these same areas have the maximum Earth visibility of above 60%. The figures also confirm the solar illumination peak sites identified in references 4, 5, 6, and 7.

These 5 coarse maps were examined for points with solar illumination peaks greater than 80% yearly average. Those points that are contiguous were given with the same site peak name, matching the site names used in Reference 5, Figure 1. Additional sites not listed in Reference 5 are given the name of the closest Site, followed by a new number, e.g. Site B from Reference 5 is listed here as sites B1, B2, and B3.

The site locations identified this way are shown in Figures 7 and 8. These sites show good correlation with the sites listed in Reference 5, but are much lower in elevation due to the different Digital Elevation Model fitting method. Sites B1, A1, and A2 also match well with the 3 peaks of maximum solar illumination identified from Clementine images in Reference 4.

Figures 9 and 10 show the north pole region. There are 7 sites with solar illumination peaks greater than 80% yearly

average. These 7 sites are marked NA through NG on the figures. The 2 best sites are NB and NC with yearly average solar illumination above 95%. Site NG has the highest average DTE communications of 96%.

### Medium Horizon Mask Results

Based on the coarse map results, 31 Medium resolution maps were generated at 40-meter resolution for the lunar south pole. These smaller 2 km x 2 km areas covered all the southern coarse map illumination peaks with greater than 80% yearly average solar illumination. Locations in 17 of the 31 Medium maps had solar illumination peaks with greater than 80% yearly average. Some solar illumination peaks that likely Digital Elevation Model processing anomalies were not considered in the final analysis.

Figures 11 and 12 show Site A1 as an example of the 2km X 2km maps. Figure 11 shows the topographic elevation contours for the map centered on (-4, -10) on Shackleton crater's West rim, containing site A1. Figure 12 is the same area covered with solar illumination contours every 10% and at 0.0001%; and Earth illumination contours at 0.0001, 0.1, 0.3, 0.5, 0.6, and 0.7%. The illumination data are for any part of the disk visible, or the "0% of solar/Earth disk visible" yearly average illumination.

Table 1 is a summary of the best average solar illumination peaks from the medium resolution maps. The following conclusions were made from examining these illumination peaks and the solar illuminations and the DTE maps:

- 1) The yearly average solar illumination maximum occurs on the highest peak in the local area. This is expected, since the tallest peak has the least obstructed view of the Sun.
- 2) At 40-meter resolution, the data show several grid points next to the illumination maximum peak with nearly the same solar illumination value. This implies the peaks are spread over several pixels, or the Digital Elevation Model data set was made self-consistent by smoothing.

Table 1. Medium View Solar Illumination Peaks Selected for Fine Resolution Analysis

Map center, X, Y km	Site Peak	X, km	Y, km	Lat., degrees	Long., degrees	Elevation, meters	Solar illum., %	Earth illum., %
-4, -10	A1	-3.72	-10.44	-89.633	-160.388	1071.74	95.58	62.49
-4, -8	A2	-3.68	-7.52	-89.723	-153.925	1050.05	94.20	63.89
-2, -4	A3	-2.20	-3.56	-89.861	-148.285	897.49	88.93	63.41
4, 2	A4	3.72	1.92	-89.861	62.700	896.57	91.46	63.99
-12, -14	B1	-12.40	-13.68	-89.388	-137.810	1260.93	97.52	65.10
-20, -10	B3	-19.96	-10.04	-89.260	-116.703	1003.61	88.63	65.52
16, -14	H	16.52	-13.08	-89.302	128.371	631.43	84.22	64.89
	C1	-38.24	13.40	-88.657	-70.688	1143.8		
	F	28.76	-21.36	-88.813	126.601	947.4		
	Malapert $\alpha$ , MA	3.56	119.60	-86.037	1.704	4206.8		
	Leibnitz $\beta$ , LB	101.32	123.04	-84.722	39.470	6054.5		

3) Within a 2km x 2km area, there are several small peaks with greater than 80% yearly average solar illumination. An area 100's of meters across may surround the actual maximum peak that also has 80% yearly average solar illumination.

4) The average Earth visibility is also maximized on these highest peaks in the site.

5) Small changes in the terrain slope (as shown in the topographic maps) greatly reduce the solar illumination, even within 100's of meters of the solar maximum peaks. This implies that finding solar maximum peaks using spacecraft pictures of illuminated terrain may be problematic. The conditions may mix light and dark terrain pixels even during the mid-Summer days. This also indicates the solar maximum peaks may not be visible on photographs due to shallow Sun angles.

6) The highest site within a region will have the greater solar illuminations. For instance, Site B1 and B3 are

located on two broad plateaus about 8 km apart. But Site B1 is about 300 meters higher, and has significantly higher average solar illumination.

Based on these observations, Sites C1 and F from Reference 5 deserved further investigation. The peaks of the two tallest mountains near the pole (Malapert  $\alpha$  and Leibnitz  $\beta$ ) were also added to the list. The peaks that were labeled Site B2 and an artifact peak near A4 were dropped from consideration. A fine resolution horizon mask was computed for the highest elevation point of each site.

#### Fine Horizon Mask Results

Fine resolution horizon mask were computed for 11 site locations in the lunar south pole region. The results of the are shown in tables 2 and 3.

Table 2. Fine resolution Solar Illumination Statistics

Site	X,km	Y,km	Average yearly illumination			months 100% visible			days dark in Winter month			days longest darkness		
			(% of Sun visible)			(% of Sun visible)			(% of Sun visible)			(% of Sun visible)		
			(0)	(50)	(100)	(0)	(50)	(100)	(0)	(50)	(100)	(0)	(50)	(100)
A1	-3.720	-10.440	93.46	90.36	86.31	4.05	2.98	1.92	8.94	12.06	15.99	2.46	2.71	5.50
A2	-3.680	-7.520	92.98	89.47	84.83	4.46	3.40	2.34	10.58	13.70	18.29	2.63	2.79	3.04
A3	-2.200	-3.560	85.36	80.75	75.22	0.05	0.00	0.00	14.03	18.37	20.43	4.92	8.86	9.19
A4	3.720	1.910	87.83	83.66	78.51	0.00	0.00	0.00	13.21	17.06	19.85	6.23	7.63	9.92
B1	-12.400	-13.680	97.01	94.79	91.67	8.02	6.96	5.90	6.32	9.59	11.73	2.79	4.10	7.54
B3	-19.960	-10.040	83.84	80.50	76.55	0.00	0.00	0.00	11.56	14.19	16.07	6.89	7.05	10.09
H	16.520	-13.080	77.53	72.20	66.57	1.60	0.53	0.00	17.39	18.95	19.85	10.42	10.74	13.78
C1	-38.240	13.400	90.01	86.95	83.12	4.29	3.23	2.17	9.27	12.22	13.94	5.33	5.90	11.31
F	28.760	-21.360	89.28	85.97	81.77	4.13	3.06	2.00	10.09	12.87	15.25	5.90	6.39	8.94
MA	3.560	119.600	83.85	80.39	76.71	1.18	0.12	0.00	11.39	12.20	13.43	11.39	11.96	12.61
LB	101.320	123.040	79.16	77.57	76.01	0.00	0.00	0.00	9.07	9.23	9.56	9.07	9.23	9.56
NB	4.200	2.400	97.57	93.85	87.95	7.36	6.30	5.24	8.61	16.08	23.46	3.20	5.41	6.40
NC	15.000	13.200	98.25	95.95	92.52	8.73	7.66	6.60	5.91	9.27	15.50	2.46	3.53	8.86
NG	12.600	-89.400	86.56	83.16	79.64	4.44	3.37	2.31	11.39	11.80	12.37	11.39	11.80	12.29

Table 3. Fine resolution Earth Visibility Statistics

Site	X, km	Y, km	Average yearly DTE Communications		
			(% of Earth visible)		
			(0)	(50)	(100)
A1	-3.720	-10.440	62.20	55.29	48.37
A2	-3.680	-7.520	63.90	56.98	50.07
A3	-2.200	-3.560	63.41	56.50	49.58
A4	3.720	1.910	63.97	57.06	50.14
B1	-12.400	-13.680	65.16	58.24	51.33
B3	-19.960	-10.040	65.60	58.69	51.77
H	16.520	-13.080	62.02	55.11	48.20
C1	-38.240	13.400	70.97	64.05	57.14
F	28.760	-21.360	67.30	60.38	53.47
MA	3.560	119.600	100.00	100.00	96.49
LB	101.320	123.040	100.00	100.00	100.00
NB	4.200	2.400	66.67	59.76	52.84
NC	15.000	13.200	71.35	64.44	57.53
NG	12.600	-89.400	96.15	91.62	85.37

The sites A1, A2, and B1 have the highest yearly average solar illumination. The other peaks do not have solar illumination metrics as good as these three peaks, primarily because of lower elevation. Site C1 is higher than sites A1 and A2, but is much farther from the south pole and therefore gets less average solar illumination.

A similar analysis was done for 3 sites at the lunar north pole identified from the coarse resolution maps. The north pole ‘fine resolution’ analysis was done using the same azimuth resolution as the south pole analysis, but was performed using only the 600-meter resolution data. These 3 sites are shown in Tables 2 and 3 as Sites NB, NC, and NG. The sites NB and NC have higher yearly average solar illumination than the lunar south pole sites, primarily because there are no obscuring peaks as tall as Malapert  $\alpha$  and Leibnitz  $\beta$  at the lunar south pole.

At the lunar south pole, Site B1 has the highest average yearly solar illumination of 97%. Site B1 also has an average Earth visibility (65%) higher than the nearby sites A1 through A4. Site B1 has the most months of continuous solar illumination, with some part of the solar disk visible during 8 synodic months. The solar power generation metrics show site B1 has the lowest total days of darkness for these 5 sites.

These solar illumination statistics are for averages of the solar motion. This allows valid site-to-site comparisons, but requires more computation for the solar illumination on specific dates. The horizon masks, like that in Figure 6, can be used with astrodynamical computations of the selenographic solar latitude and longitude to find the illumination metrics for specific dates. Since the horizon masks don’t vary with time, only the solar motion computations are required for this next level of analysis.

The average yearly Earth visibility metrics of Table 3 indicate little variation between the sites on the rim of Shackleton Crater. In general, the best visibility of any part of the Earth is around 65% for the lunar Polar Regions. From these peaks, the entire Earth is visible about 50% of the sidereal month. Therefore, continuous polar lunar base coverage requires some kind of Earth relay. The sites on the peaks of Malapert  $\alpha$  and Leibnitz  $\beta$  have 100% visibility of Earth at all times (Figure 13). These sites also have direct line-of-sight to the rim of Shackleton crater. This makes possible a communications system design using a radio frequency reflector at one of these sites as a continuous relay between Earth and sites on the rim of Shackleton crater. For the lunar north pole, site NG on the North rim of Peary Crater has 96% visibility of Earth. This site could provide a near continuous relay between Earth and sites NB and NC near the lunar south pole.

#### *Using Towers to Improve Metrics*

Solar illumination and Earth visibility metrics increase with increased altitude above the local terrain. The following equations show this variation as a function of altitude and distance from the pole. The equations assume a spherical lunar surface of radius,  $R$ , an altitude above this surface,  $h$ , and a distance from the pole,  $d$ . The equations are written in terms of colatitude,  $\theta$ , and below-the-horizon view angle,  $\phi$ , given by the following equations.

$$\theta = \frac{d}{R} \times \frac{180}{\pi} \quad (1)$$

$$\phi = \arccos\left(\frac{R}{R+h}\right) \quad (2)$$

The equations for the yearly averages were derived by integrating along the local horizon in lunar latitude-longitude coordinates. The derivation uses an approximation for small angles that gives equation 3. This equation is valid for small angles near the polar regions.

$$longitude \approx \arccos\left(\frac{-\phi - latitude}{\theta}\right), \quad (3)$$

$$latitude \approx -\phi - \theta \cos(longitude)$$

Integrating the area above the horizon mask and between the solar latitude limits produced an equation for the yearly average solar illumination. The solar latitude limits are +and-1.54 degrees, represented by +and  $-\alpha$  below. The equation uses the variables  $L1$  for the longitude where the horizon mask crosses  $-\alpha$  latitude, and  $L2$  for the longitude where the horizon mask crosses  $+\alpha$  latitude. These variables are:

$$L1 = \begin{cases} \text{if } (\theta + \phi) \geq \alpha, & \arccos\left(\frac{-\phi + \alpha}{\theta}\right) \\ \text{else,} & 0 \end{cases} \quad (4)$$

$$L2 = \begin{cases} \text{if } (\theta - \phi) \geq \alpha, & \arccos\left(\frac{-\phi - \alpha}{\theta}\right) \\ \text{else,} & 180 \end{cases}$$

The yearly average solar illumination,  $I$ , is then given by the equation:

$$I = \frac{L1}{180} + \frac{(\alpha + \phi)(L2 - L1)}{360 \times \alpha} + \frac{\theta}{2\pi\alpha} [\sin(L2) - \sin(L1)] \quad (5)$$

Integrating the area above the horizon mask and between the Earth latitude limits produced the yearly average Direct to Earth communication equation. The Earth latitude limits are +and-6.87 degrees, represented by +and  $-\gamma$  below. The Earth longitude limits of +and -8.16 degrees are represented by +and  $-\beta$  below. The equation uses the variable  $L0$  for

the longitude of the site at Cartesian coordinates (x,y) centered on the pole. The equation uses the variable L1 for the longitude where the horizon mask crosses  $-\beta$  latitude. These variables are:

$$L0 = abs[\arctan(x/y)]$$

$$L1 = \begin{cases} \text{if } (\theta + \phi) \geq \gamma, & \arccos\left(\frac{-\phi + \gamma}{\theta}\right) - L0 \\ \text{else,} & -\beta \end{cases} \quad (6)$$

The yearly average Earth communications, DTE, is then given by the equation:

$$DTE = \frac{1}{4\gamma\beta} \left\{ \begin{array}{l} 2\gamma(L1 + \beta) + (\gamma + \phi)(\beta - L1) \\ + \theta \frac{180}{\pi} [\sin(\beta + L0) - \sin(L1 + L0)] \end{array} \right\} \quad (7)$$

Comparing these theoretical equations with the computed illumination and DTE communications averages required using an adjusted lunar reference altitude at the poles. The lunar reference geoid radius of 1738 km is not a good average value for the terrain at either pole. The lunar south pole is part of the Aitken Basin, and the GSSR Digital Elevation Model elevations have an average of -1880 m within 200 km of the south pole. The lunar north pole region has an average elevation of -1673 m within 150 km of the north pole. These averages were subtracted from base site reference altitude to get the value of 'h' used in equation 2. This effectively gives the base sites a higher elevation relative to the local average elevation.

For selected base sites, solar illumination and DTE communications averages were computed for tower heights from 2 m to 1500 m, and in some cases 3000 m. Then these tower heights plus adjusted altitudes and base locations were used in equations 1 through 7 to get predicted values of the yearly average metrics. The results are shown in figures 14 and 15. Figure 14 shows black curves of equation 5 plotted parametrically with distance from the pole. For the selected sites, the computed yearly average solar illumination is shown by squares, connected by a dashed line with the theoretical yearly average for the same location and tower heights. The theoretical values are marked with X's. South lunar Pole sites are in blue and the lunar north pole sites are in red. The plots show reasonable agreement of computed values and theory, with the computed value never exceeding the theoretical. Figure 15 shows black curves of equation 7 plotted parametrically with distance from the pole. The value of L0 was set to zero for the parametric curves. Figure 15 include computed and theoretical values of the yearly average DTE communications for the same sites as figure 14, using the same symbol and color conventions.

At no site will a tower of 1500 m or less provide both 100% average yearly solar illumination and 100% average DTE

communications. Towers of 1500 m at sites NB and NC will raise the average yearly solar illumination to 100%. But for the lunar south pole sites, like B1, towers of over 2500 m are required to raise the average yearly solar illumination to 100%. This is because the peaks Malapert  $\alpha$  and Leibnitz  $\beta$  obscure the view of the sun from the lunar south pole. Equation 8 gives the elevation, Hp, above a spherical surface needed to see the winter sun over a peak of elevation Hm at a distance, d, from the pole. Equation 8 provided values in Figures 4 and 14 for the Malapert  $\alpha$  and Leibnitz  $\beta$  peaks.

$$Hp = (R + Hm) \frac{\cos\left(\frac{180}{\pi} \frac{d}{R} - \alpha\right)}{\cos(\alpha)} - R \quad (8)$$

The obscuring effect of these peaks is also shown in figure 5, where the peak Malapert  $\alpha$  is at +10 degrees azimuth.

Figure 15 shows the yearly average DTE communication varies more with distance from the pole toward the prime meridian that with tower height above the local terrain. Towers up to 3000 m at the poles do not make significant improvements in the DTE communications average. The computed yearly average DTE communications for site NG exceed the predicted values for towers between 32 and 1500 meters tall. This is because the view northward from site NG toward the Earth looks across the floor of Byrd Crater, which averages about -2500 m elevation.

#### Considerations for Photovoltaic Array Design

The lunar pole sites create some difficult challenges for designing a continuously operating photovoltaic power system. A site with continuous solar illumination will see the Sun travel through 360 degrees of azimuth during 1 synodic month. A photovoltaic power system would require several permanently mounted photovoltaic arrays pointed in several directions, or would have to continually track the Sun with a single array. Since a single array requires much less mass, the design of the solar tracking system is examined here.

The requirement to continually track the Sun could be met by installing the photovoltaic array on a vertical axle, oriented parallel to the lunar spin axis. At the lunar south pole, this axle would rotate counterclockwise with the Sun to keep the array normal to the solar radiation. This requires a foundation to support the axle, cross beam structures to hold the array on the axle, and a drive system to turn the array. This system also requires a solution to the 'cable wrap' problem, in order to continually track the Sun. After 1 synodic month the array has turned through 360 degrees, and needs to continue rotating in the same direction. Power and control cables from the array need to go through multiple slip rings, or the array needs to rotate 360 degrees clockwise to unwrap the cables. A slip ring design is further complicated by the requirement to tolerate the fine dust on

the lunar surface. Using the ‘cable unwrap’ method means stopping power production for a short amount of time, once per synodic month.

A heliostat design using a focusing mirror may provide a low-mass solution to the ‘cable wrap’ problem [Ref 10]. Figure 16 shows a photovoltaic array installed horizontal to the local terrain. A parabolic section mirror is installed above the array, angled at approximately 45 degrees to the local horizontal. This mirror is suspended from the crossbar of a mast placed next to the array. The mast could also be the structure for the Lunar Communications Terminal (LCT) antennas. The mirror is suspended from an axle that is oriented parallel to the lunar spin axis and rotates once per synodic month to continually reflect solar radiation onto the array. The mirror can continue to track after 360 degrees revolution, since there are no cables attached to the moving part. This heliostat ‘periscope’ design provides continuous solar tracking, but is partially shaded once per revolution when the Sun passes behind the support mast.

Shaping the mirror into a parabolic arc concentrates solar power for a small increase in mass. The tradeoffs should consider the relative mass-per-unit area of the mirror and the photovoltaic panels, the reflectivity of the mirror material, and the relative masses of an array-support axle versus a mirror heliostat axle plus mast.

Additional flat ‘periscope’ mirrors mounted on the crossbar could be used to direct solar light to areas nearby. This provides an efficient method of lighting work areas because it bypasses the inefficiencies of the photovoltaic system, battery storage, and electric lighting. If the photovoltaic power system is located on a crater rim (as in Figure 16), a flat ‘periscope’ mirror could provide continuous lighting to exploration crews in the permanently shadowed areas within the crater. Sufficiently large heliostat mirrors could redirect enough sunlight to run photovoltaic arrays at remote locations. This would provide very efficient power transfer for operating within the permanently shaded areas.

## 5. CONCLUSIONS

Separating the lunar pole solar illumination problem into terrain horizon mask and solar motion computations simplified the production of illumination metrics. Using a simplified model of average solar motion allowed quick comparisons between lunar south pole sites. The results show that within 100 km of the lunar south pole, solar illumination is maximized at previously identified site locations. These sites are small areas on the peaks of isolated mountains and crater rims. No site provides 100% yearly average for both solar illumination and DTE communication. Lunar north pole sites were also examined. No site at either pole provides 100% yearly average for solar illumination unless a tower at least 1500 m is placed on one of the best lunar north pole sites.

The best lunar south pole sites are on the rim of Shackleton crater, and the ridge west of Shackleton crater. These 3 sites have yearly average of solar illumination between 93 and 97%. The Sites have 100% solar power generation capability about 85 to 92% of the year. For both of these metrics, Site B1 on the ridge West of Shackleton crater has the highest solar illumination values. Site B1 has direct-to-Earth visibility of the entire Earth disk about 51% of each month. More detailed analysis of site B1 can use the terrain horizon masks presented here, coupled with more detailed true-of-date solar motion computations.

Examination of the site solar illumination profiles at 40-meter resolution shows the peaks of illumination are distributed over many points. The locations with greater than 80% solar illumination are spread over 100s of meters. This supports the conclusion that the Digital Elevation Model has adequate sampling to show the true terrain characteristics.

The lunar north pole base sites NB and NC have yearly average solar illumination around 97%, and have 100% solar power generation capability about 88 to 92% of the time for the average year.

The yearly average for 100% DTE communications at the best lunar north pole and south pole sites are all around 50%. The yearly average DTE communications does not vary significantly with tower height, but does increase to 100% for sites about 100 km from the poles toward the lunar prime meridian.

## 6. ACKNOWLEDGMENTS

This research was carried out at the Jet Propulsion Laboratory, California Institute of Technology, under a contract with the National Aeronautics and Space Administration.

The author expresses thanks to Martin A. Slade of JPL’s GSSR group for his time and assistance with the 2006 GSSR Digital Elevation Model data. The author also wished to thank Charles Ruggier and Laif Swanson of the SCiP Study Team at JPL for their support of this work.

## REFERENCES

1. Scott Hensley, Eric Gurrola, Paul Rosen, Martin Slade, Joseph Jao, Micheal Kobrick, Raymond Jurgens, Eric De Jong, and Barbara Wilson, “RADAR generates high-resolution topographic map of the Moon”, Society of Photo-Optical Instrumentation Engineers Newsroom, June 16, 2008.
2. J. L. Margot, D. B. Campbell, R. F. Jurgens, M. A. Slade, “Topography of the Lunar Poles from RADAR

Interferometry: A Survey of Cold Trap Locations”, Science, Vol 284, pg 1658-1660, 4 June 1999.

3. NASA, “The Vision for Space Exploration”, Feb. 2004. [http://www.nasa.gov/pdf/55584main\\_vision\\_space\\_explorat ion-hi-res.pdf](http://www.nasa.gov/pdf/55584main_vision_space_explorat ion-hi-res.pdf).

4. M. Kruijff, “The Peaks of Eternal Light on the Lunar South Pole: How they were found and what they look like”, 4th International Conference on Exploration and Utilization of the Moon (ICEUM4), ESA/ESTEC, SP-462, September 2000.

5. J. Fincannon, “Lunar South Pole Illumination: Review, Reassessment, and Power System Implications”, 5<sup>th</sup> International Energy Conversion Engineering Conference and Exhibit (IECEC), 25-27 June 2007, AIAA 2007-4700.

6. J. Fincannon, “Characterization of Lunar Polar Illumination From a Power System Perspective”, 56<sup>th</sup> AIAA Aerospace Sciences Meeting and Exhibit, 7-10 January 2008, AIAA 2008-0447.

7. M. Zuber, I. Garrick-Bethell, “What Do We Need to Know to Land on the Moon Again?”, Science, Vol 310, pg 983-985, 11 November 2005.

8. Gazetteer of Planetary Nomenclature, International Astronomical Union, 03/31/2008

9. Ewan A. Whitaker, “The Lunar South Polar Regions”, Journal of the British Astronomical Association, Vol. 64, No. 6, pp. 234-242.

10. James D. Burke, “Merits of A Lunar Polar Base Location”, Lunar Bases and Space Activities of the 21st Century. Houston, TX, Lunar and Planetary Institute, edited by W. W. Mendell, 1985, p.77.

## BIOGRAPHY

**Scott H. Bryant** is a member of the senior staff at the Jet Propulsion Laboratory. He has a bachelor’s in Aeronautics and Astronautics Engineering from MIT and a master’s in Astronautics from USC. He has worked for the Jet Propulsion Laboratory for over 10 years, working on several of JPL’s Deep Space Network (DSN) systems. His projects include the receivers, exciters, and spacecraft tracking subsystems. He has been principally involved with software design and development for spacecraft tracking, including holding the position of cognizant design engineer for the current DSN Ranging system. Scott is currently the implementation and design lead for the spacecraft tracking and ranging portion of JPL’s Network Simplification Project. He has also worked with the study groups examining communications and navigation issues for the Constellation system lunar studies. The work presented here was performed for the SCiP Lunar Architecture study group.

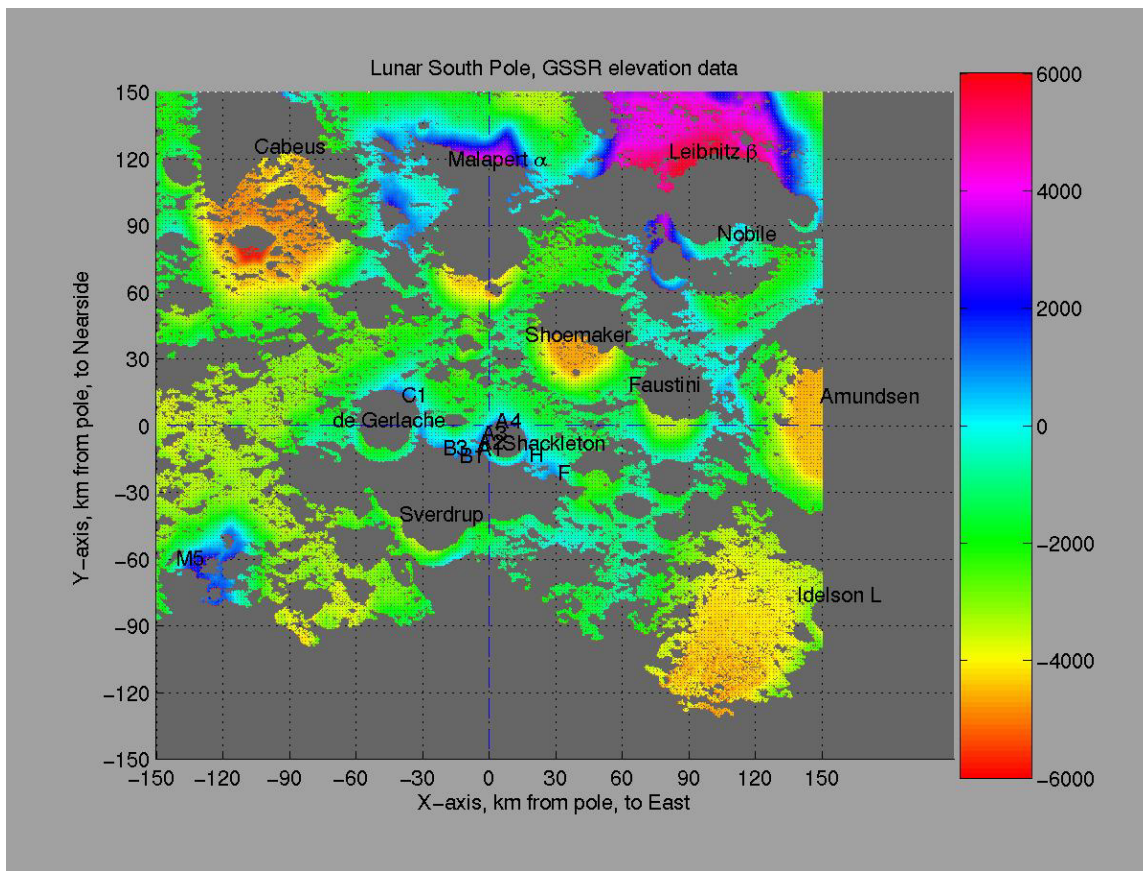


Figure 1: Lunar South Pole Elevation Map from GSSR 2006 Digital Elevation Model.

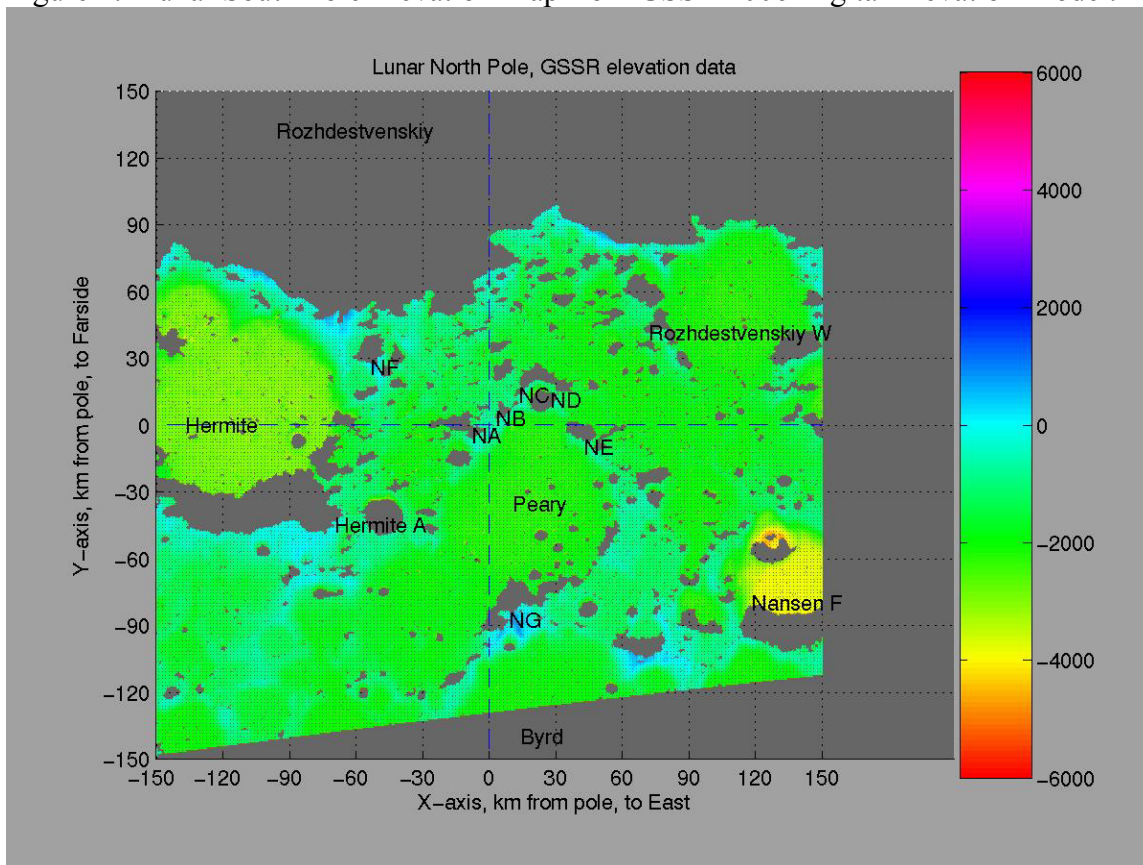


Figure 2: Lunar North Pole Elevation Map from GSSR 1997 Digital Elevation Model.

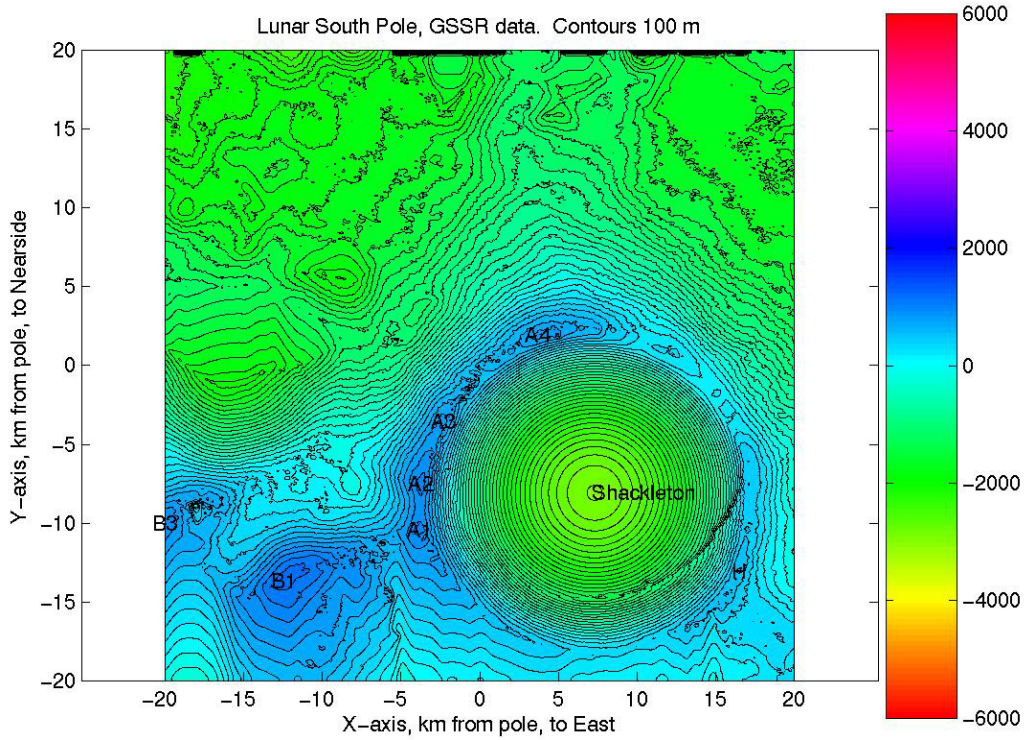


Figure 3: Shackleton Crater Topographic Map, with Base Sites.

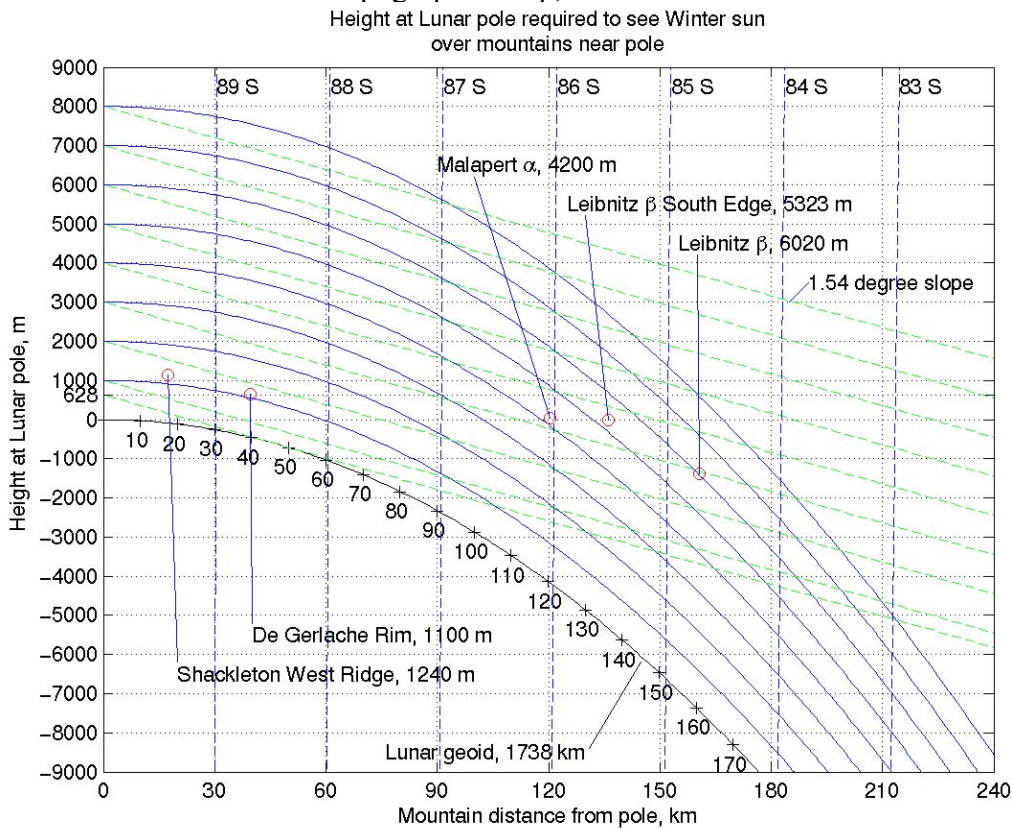


Figure 4: Solar Lines-of-Sight at Lunar South Pole

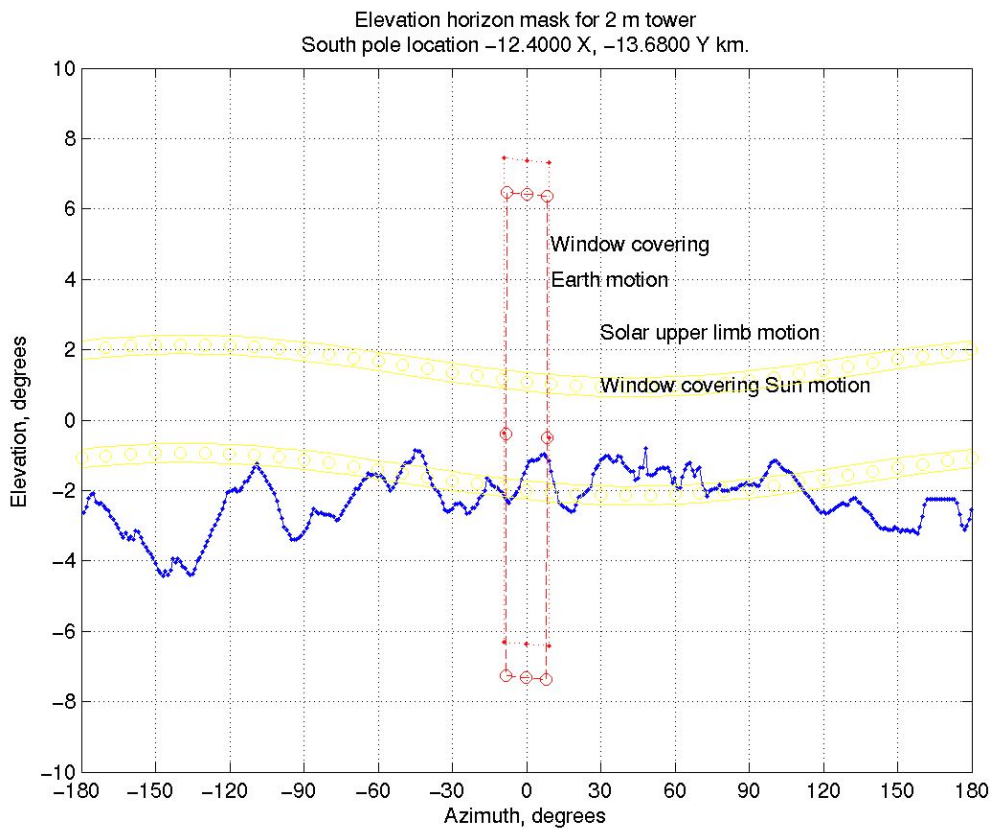


Figure 5: Site B1 Terrain horizon mask with 1 degree azimuth spacing.

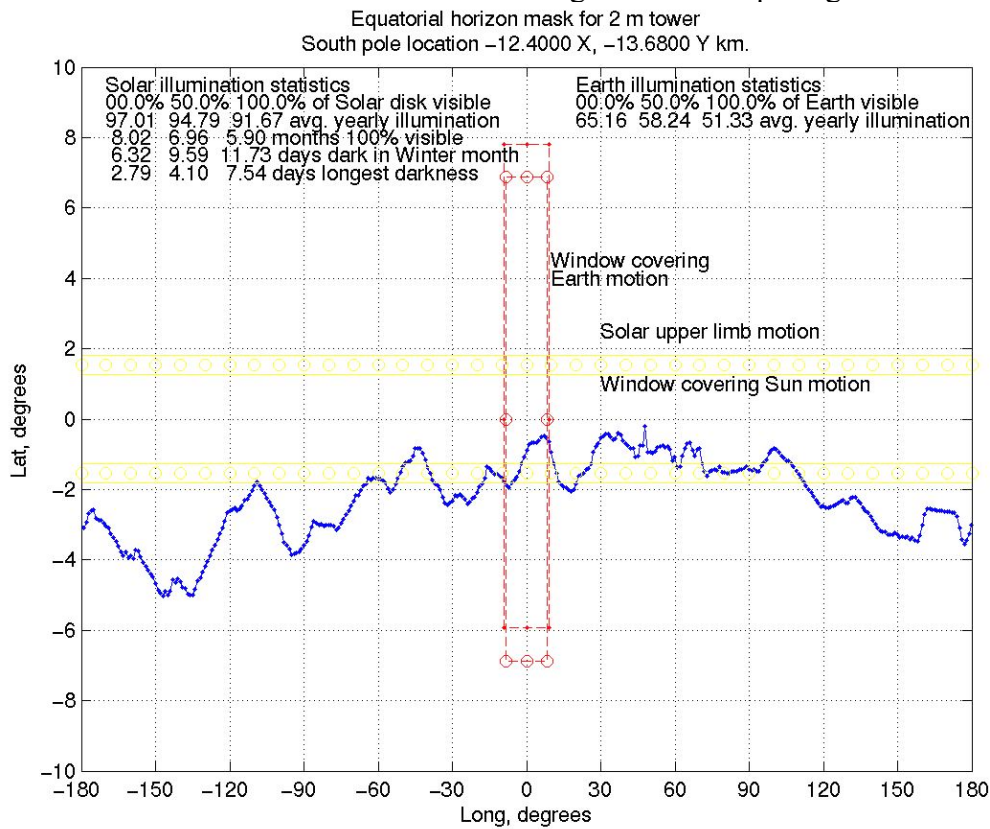


Figure 6: Site B1 Terrain horizon mask with 1 degree azimuth spacing, in equatorial coordinates.

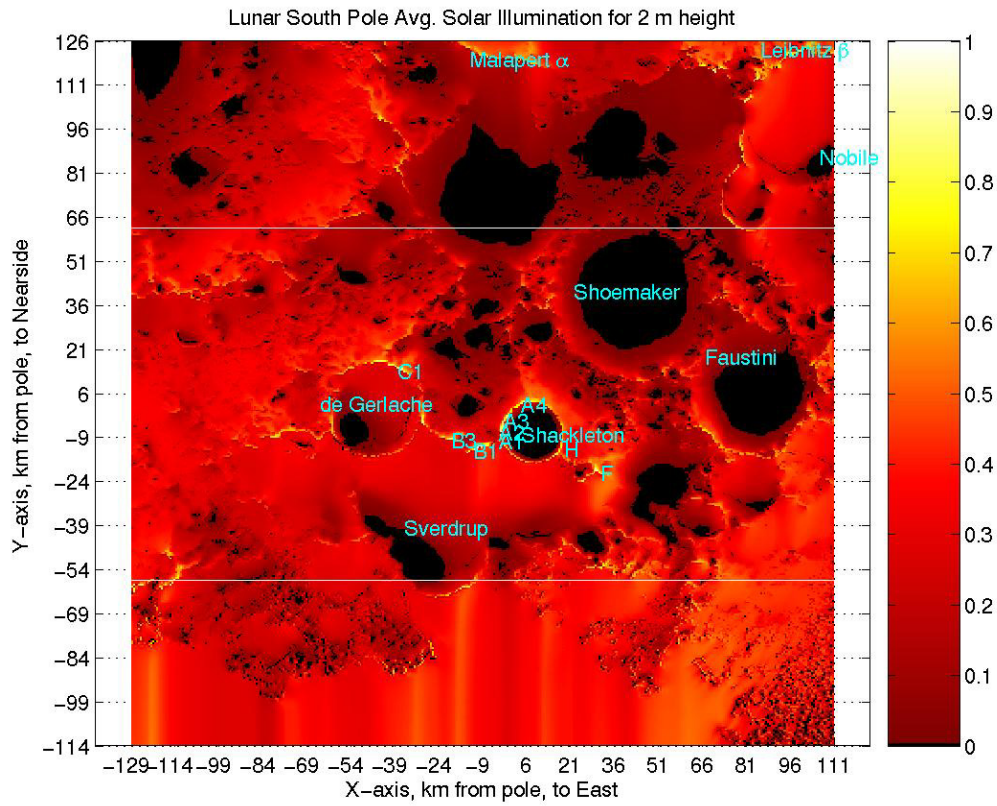


Figure 7: Lunar South Pole Solar Illumination Yearly Average.

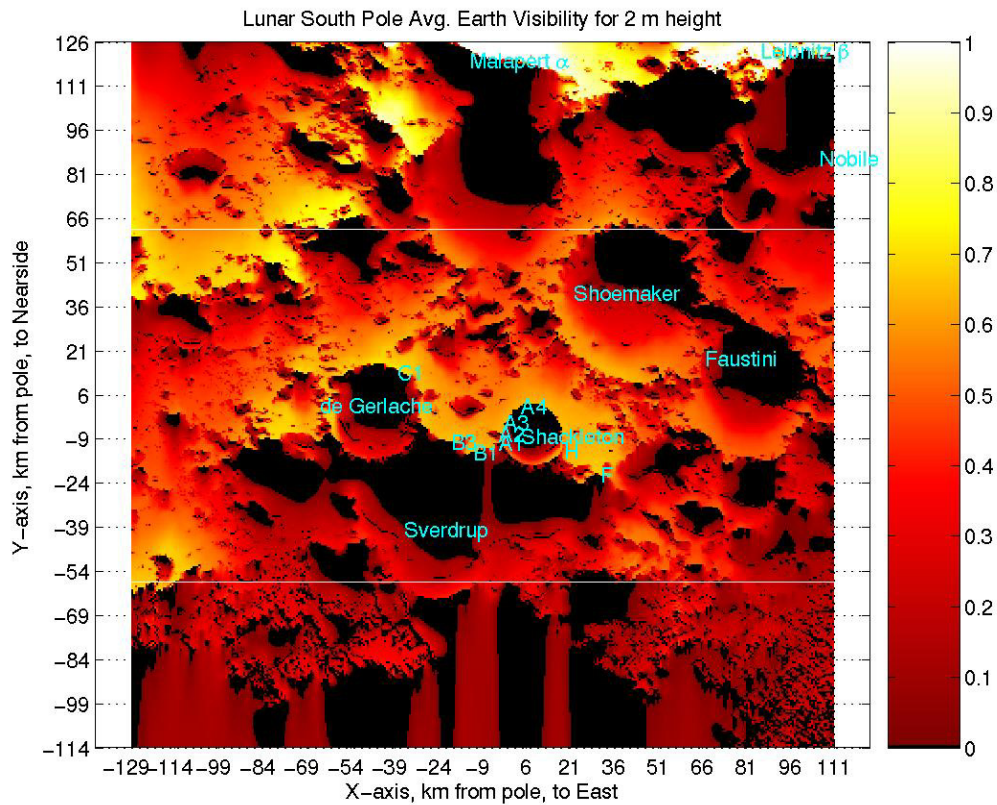


Figure 8: Lunar South Pole DTE Visibility Yearly Average.

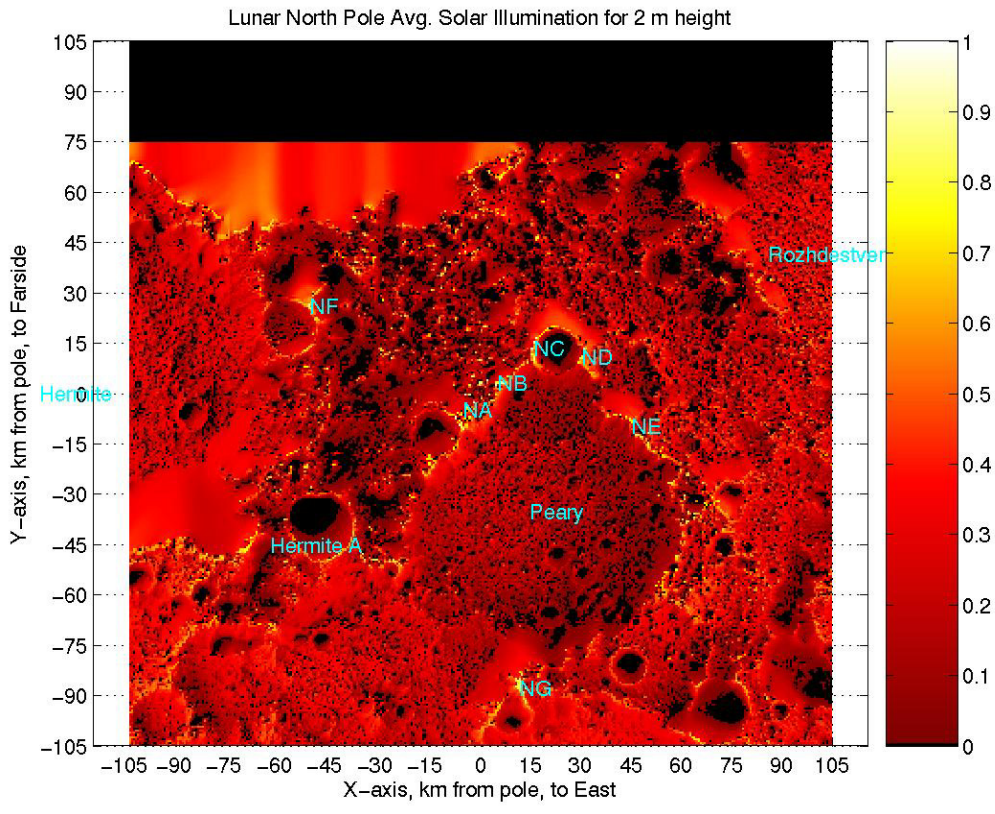


Figure 9: Lunar North Pole Solar Illumination Yearly Average.

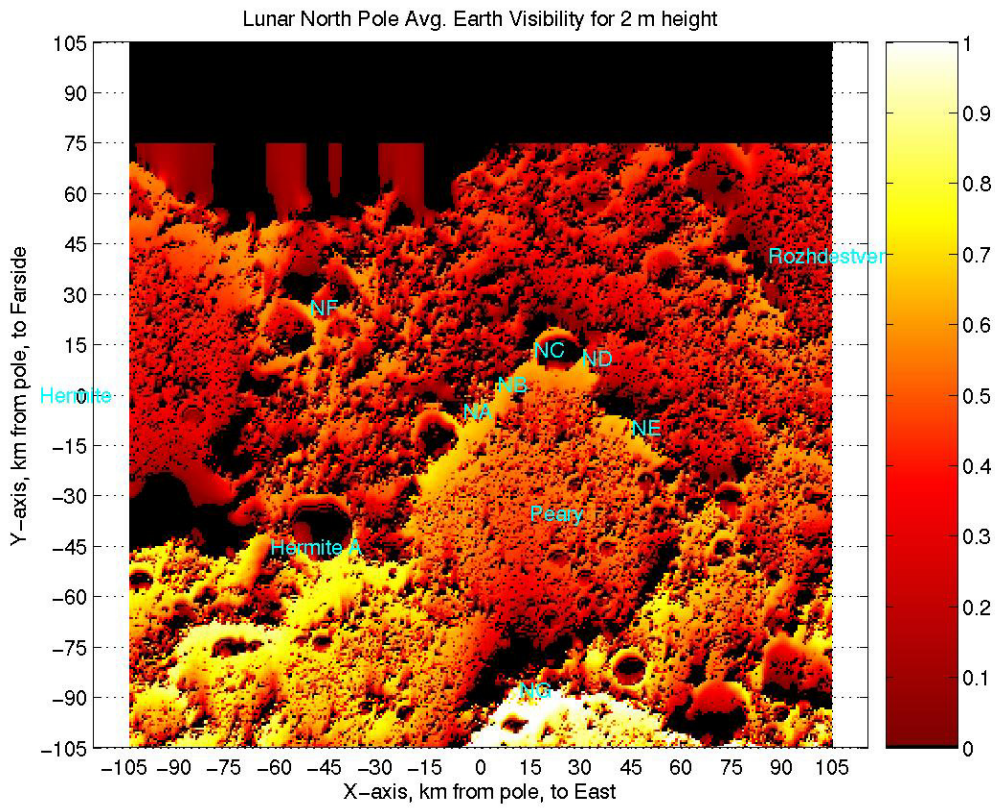


Figure 10: Lunar North Pole DTE Visibility Yearly Average.

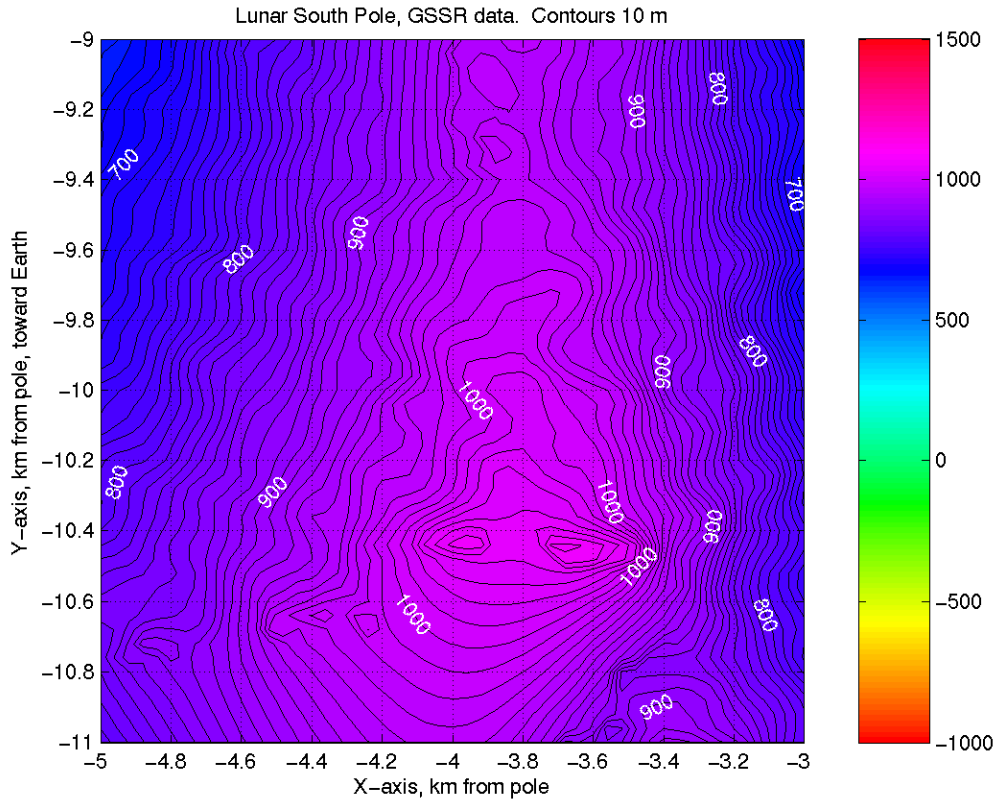


Figure 11: Site A1 Elevation Topography.

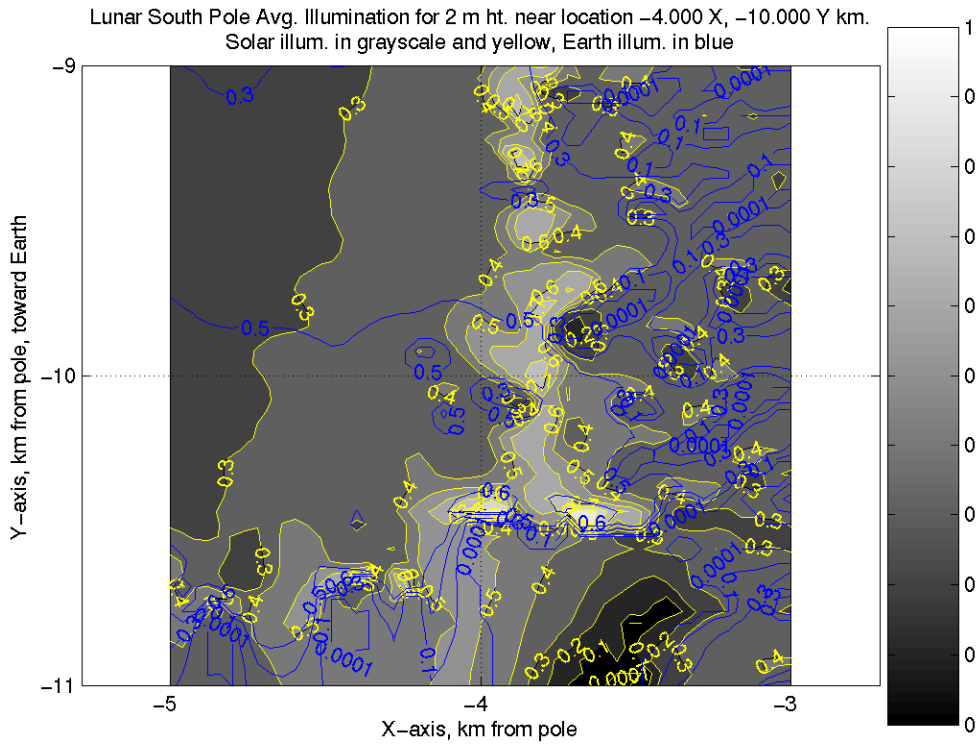


Figure 12: Site A1 Yearly Average Solar Illumination and DTE visibility, Medium Resolution.

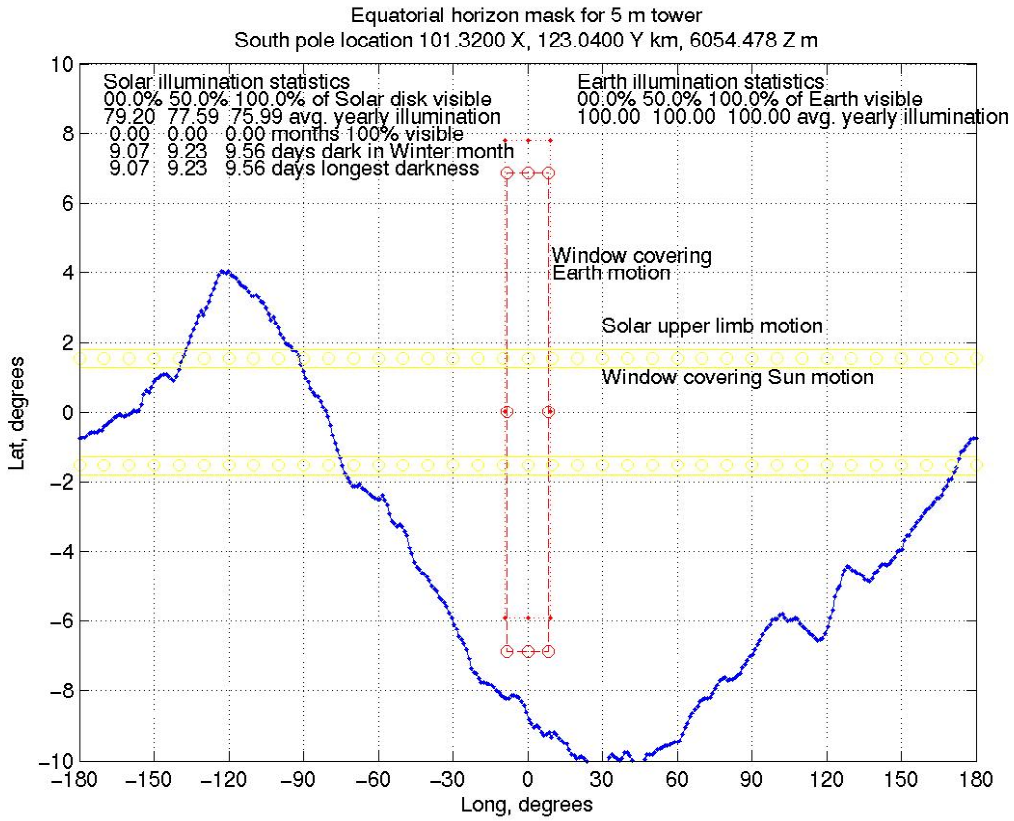


Figure 13: Site LB Terrain Horizon Mask.

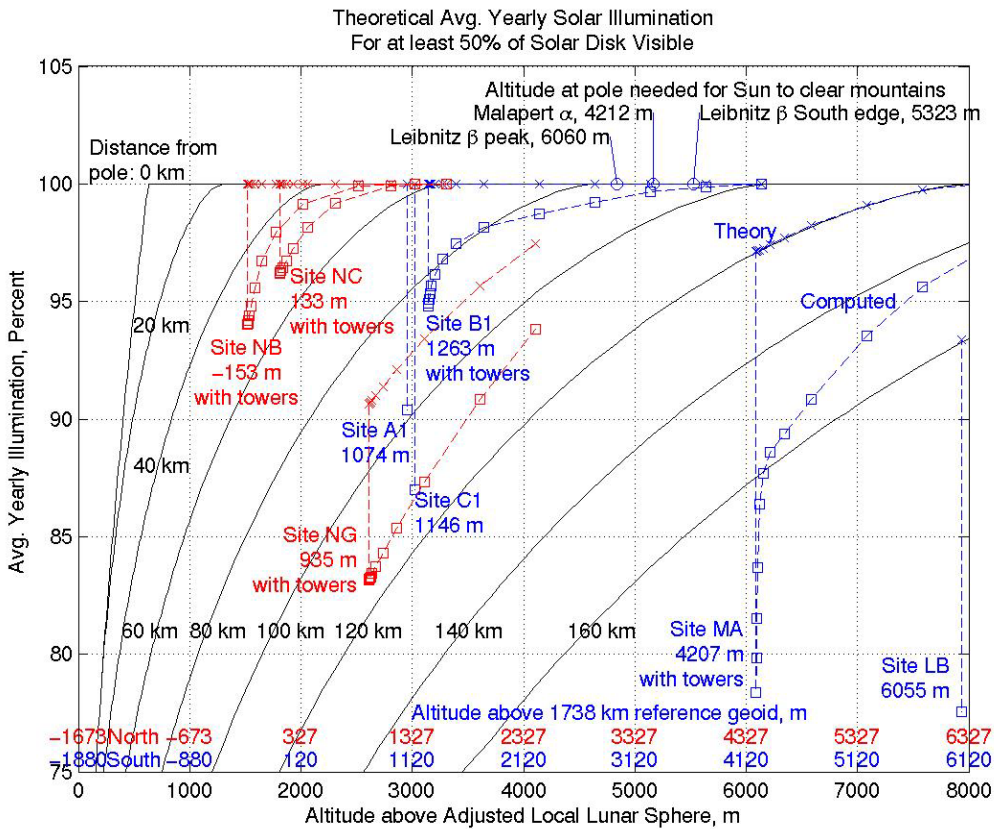


Figure 14: Theory and Computed values of Average Yearly Solar Illumination.

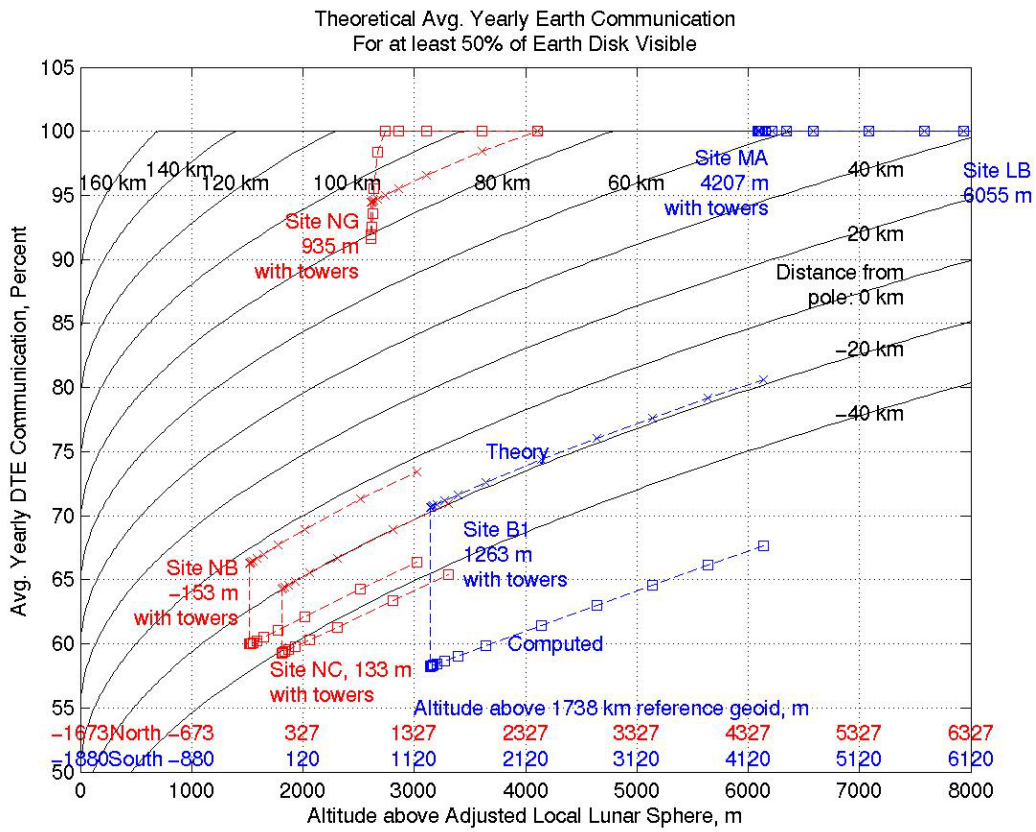


Figure 15: Theory and Computed values of Average Yearly DTE Communication.

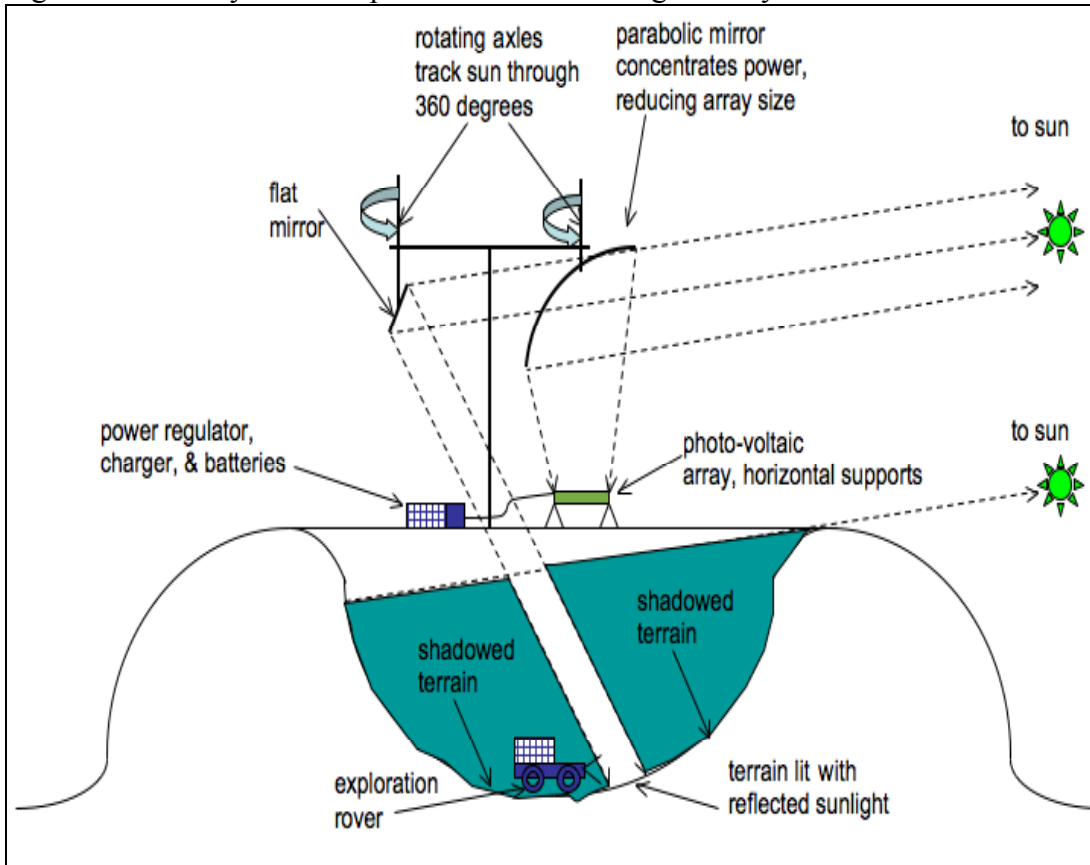


Figure 16: Heliostat Mirror Design to Eliminate Cable Wrap.